Journal of Aircraft (2012). 49(1), 341-348.
DOI: http://dx.doi.org/10.2514/1.C031490

Framework for Aircraft Trajectory Planning Toward an Efficient Air Traffic Management

M. Soler,* A. Olivares,† and E. Staffetti‡
Rey Juan Carlos University, 28933 Móstoles, Spain

* Research Engineer and Ph.D. Candidate, Department of Statistics and Operations Research; manuel.soler@urjc.es. Student Member AIAA.
† Associate Professor, Department of Signal Theory and Communications; alberto.olivares@urjc.es. Member AIAA.
‡ Associate Professor, Department of Signal Theory and Communications; ernesto.staffetti@urjc.es.

D. Zapata§
Airbus Military, 28906 Getafe, Spain

§ Research Engineer, Division of Engineering and Technologies; daniel.zapata.external@military.airbus.com

I. Introduction

THE current air traffic management (ATM) is a complex, highly regulated, and inefficient system [1]. The improvement of such an ATM paradigm is a challenging research area for the air transportation community [2]. One of the main goals pursued is to decrease aircraft emissions and fuel consumption in flight profiles. In particular, single European sky ATM research (SESAR) pursues the following by 2020: 8–14 min gain per flight on average, 300–500 kg reduction in fuel per flight on average, and 945–1575 kg reduction of CO_2 emissions per flight on average [3].

The SESAR concept of operations requires a paradigm shift from a highly structured and fragmented system, heavily reliant on tactical decision and with few strategic planning functions, to an integrated one based on collaborative strategic management of trajectories [4]. In the future European ATM system to be built under SESAR, the trajectory becomes the key piece of a new set of operating procedures referred to as trajectory-based operations (TBO) [5]. Therefore, the strategic-level implementation of optimal four-dimensional trajectories must be done within an intricate framework of increasing complexity.

In the flight of an aircraft, several flight phases can be distinguished for climbing, cruising, and descent, each with an associated dynamic model and a set of path constraints. Thus, multiple flight models can be used for different phases to solve a so-called multistage or multiphase trajectory optimization problem [6–8].

This Note solves a multiphase trajectory optimization problem using the methodology presented in [9]. The idea is that the flight of an aircraft has intrinsically got the characteristics of a controlled switched dynamic system. Then, the authors combine all phases making a sequence and, by a parametrization of the switching instants, convert the multiphase optimal control problem into a conventional optimal control problem. For details, mathematical background, and general references on multiphase optimal control, the reader is referred to [9] and references therein.

In the scope of trajectory planning, recent widespread activity in ATM research has been done toward greener operational concepts. Departure procedures for minimizing noise nuisance have been analyzed [10–13]. Analysis of minimum fuel cruise at constant altitude has been done [14,15], showing that the steady cruise is far from the optimal. Arrival operations have also been studied, with special focus on continuous descent approach (CDA), obtaining important fuel savings, and environmental benefits when putting it into practice in real scenarios [16–18]. Optimal trajectories with airspace constraints have also been discussed [19].

However, more efforts on trajectory optimization are needed to analyze performances, propose procedures, and set standards. With this aim, this Note presents a framework for commercial aircrafts strategic four-dimensional trajectory planning toward a TBO concept of operations.

Within this framework, the authors define what are termed optimized procedured profiles. They are based on a relaxation of current procedures by setting, in general, just one procedure per phase and relaxing some trigger conditions of switching between phases. To evaluate such a methodology, short- and medium-range vertical optimized procedured profiles are compared with fully procedured profiles, those used in the current paradigm, which can be consulted in [20], and free-flight profiles, considered as optimal performance benchmarks. Aircraft performances, flight procedures, and the resulting consumptions are analyzed and discussed.

II. Methodology and Framework

A switched dynamic system is composed of a set of dynamic systems:

$$\dot{x} = f_k[x(t), u(t), t], \qquad k \in \{0, 1, \ldots, N\} \tag{1}$$

where x represents the n-dimensional state vector, the set $\{0, 1, \ldots, N\}$ represents the different dynamic systems, and a switching sequence in $[t_I, t_F]$, defined as the timed sequence of $N + 1$ active dynamic systems,

$$\sigma = [(t_I, k_I), (t_1, k_1), \ldots, (t_N, k_N)] \tag{2}$$

where $0 \leq N < \infty$, $t_I \leq t_1 \cdots \leq t_N \leq t_F$, and $k_j \in \{0, 1, \ldots, N\}$. To control a switched dynamic system, both a m-dimensional control input, $u(t)$, and a switching sequence, σ, have to be specified.

Consider the switched dynamic system (1) whose state and control variables are subjected to a set of equality and inequality constraints:

$$g_k[x(t), u(t), t] = 0, h_k[x(t), u(t), t] \leq 0, \qquad k \in \{0, 1, \ldots, N\} \tag{3}$$

Given an initial state, $x(t_I)$, a final state, $x(t_F)$, a time interval, $[t_I, t_F]$, and a prescribed untimed sequence of active dynamic systems, $\zeta = (k_I, k_1, \ldots, k_N)$, we study the problem of finding a piecewise continuous input, $u(t)$, the switching instants, $(t_1, \ldots, t_N)$, and the corresponding piecewise smooth trajectory, $x(t)$, between $x(t_I)$ and $x(t_F)$, that fulfil Eqs. (1) and (3), and minimize

$$J = \phi[x(t_F)] + \int_{t_I}^{t_F} L[x(t), u(t), t]\,\mathrm{d}t \tag{4}$$

The final time, t_F, may be fixed or left free. We assume that f_k, g_k, h_k, and ϕ are smooth enough functions.

We then introduce the new independent variable, $\tau \in [0, 1]$, as in [9]. By introducing the new independent variable, τ, the evolution equation on the interval $[t_k, t_{k+1}]$ given by Eq. (1) becomes

$$x' = (N+1)(x_{n+k+1} - x_{n+k})\hat{f}_k(x, u, \tau) \tag{5}$$

where $(\cdot)'$ denotes the derivative of $(\cdot)$ with respect to the new independent variable, τ, and

$$\hat{f}_k(x, u, \tau) = f_k[x, u, t(\tau)]$$

Let $\hat{x}$ be the extended state vector

$$\hat{x} = [x_1, \ldots, x_n, x_{n+1}, \ldots, x_{n+N}]^T$$

where the new state variables, $x_{n+1}, \ldots, x_{n+N}$, correspond to the switching times, t_k, $k \in \{1, 2, \ldots, N\}$, i.e., $x_{n+k} = t_k$, with $\dot{x}_{n+k} = 0$.

Then, define on each interval $k/(N+1) < \tau \leq (k+1)/(N+1)$:

$$\hat{L}(\hat{x}, u, \tau) = (N+1)(x_{n+k+1} - x_{n+k})L[x, u, t(\tau)]$$

We can rewrite the functional (4) as

$$\begin{aligned}\hat{J} &= \phi[\hat{x}(1)] + \int_0^{\frac{1}{N+1}} \hat{L}(\hat{x}, u, \tau)\,\mathrm{d}\tau + \cdots + \int_{\frac{N}{N+1}}^1 \hat{L}(\hat{x}, u, \tau)\,\mathrm{d}\tau \\ &= \phi[\hat{x}(1)] + \int_0^1 \hat{L}(\hat{x}, u, \tau)\,\mathrm{d}\tau \end{aligned} \tag{6}$$

and the task is to minimize $\hat{J}$ in the extended state space, subject to Eq. (5) in the reformulated problem, and to the corresponding path constraints in Eq. (3). The new equivalent problem is a conventional optimal control problem. The last N components of the optimal solution of this problem, $\hat{x}^*$, will be the optimal switching times t_k, $k = 1, \ldots, N$. The reformulated optimal control problem is stated as follows:

$$\min \hat{J} \tag{7}$$

$$\text{Subject to } x' = (N+1)(x_{n+k+1} - x_{n+k})\hat{f}_k(x, u, \tau), \quad \text{dynamic constraint} \tag{8}$$

$$x'_{n+1} = \ldots = x'_{n+N} = 0, \qquad \text{switching dynamic constraint} \tag{9}$$

$$x(t_I) = x_{t_I}, \qquad \text{initial-boundary condition} \tag{10}$$

$$\psi[x(t_F), t_F] = 0, \qquad \text{final-boundary condition} \tag{11}$$

$$\phi_{l_k} \leq \phi_k(x, u) \leq \phi_{u_k}, \qquad \text{path constraints} \tag{12}$$

Notice that Eqs. (8), (9), and (12) correspond to the set of equality and inequality constraints in Eq. (3).

In this framework, flight plans are modeled as a collection of phases (in figures labeled Ph), connected by end trigger (ET) conditions which make the system switch between one phase and the following. The discrete states of the flight plan model are stored in the following variables: flight phase (Ph), aerodynamic configuration (AC), dynamic mode (DM), operational procedure (OP), and atmosphere mode (AM), so that $\hat{f}_k = \xi(\mathrm{Ph}_k) = \xi(\mathrm{AC}_k, \mathrm{DM}_k, \mathrm{OP}_k, \mathrm{AM}_k)$. When $\{\mathrm{ET}_k\}_{k=0,\ldots,N-1}$ is triggered, the system switches form k to $k+1$ (see Fig. 1). Flight phase mode, $\mathrm{Ph} \in \{0, \ldots, N\}$, represents the phases constituting the flight plan. The AC mode represents the flap configuration of the aircraft. Generally, five different AC can be distinguished: takeoff (TO), initial climb (IC), cruise (CR), approach (AP), and landing (LD). Thus, $\mathrm{AC} \in \{\mathrm{TO}, \mathrm{IC}, \mathrm{CR}, \mathrm{AP}, \mathrm{LD}\}$. Whether the aircraft flies in a configuration depends upon either a threshold altitude, $H_{T_{(\cdot)}}$, or a stall speed, $V_{S_{(\cdot)}}$ (see Fig. 2). The DM, $\mathrm{DM} \in \{3\mathrm{D}, \mathcal{H}, \mathcal{V}\}$, represents, respectively, either purely three-dimensional, horizontal ($\mathcal{H}$), or vertical ($\mathcal{V}$) ordinary differential equations (ODE) systems governing the motion of the aircraft. OPs can be also specified. $\mathrm{OP} \in \{\mathrm{PATH}, \mathrm{CAS}, M, T_{\max}, T_{\min}, \mathrm{HO}\}$ represents, respectively, a constant flight-path angle procedure (labeled PATH), a constant calibrated airspeed procedure (labeled CAS), a constant Mach procedure (M), a maximum thrust procedure ($T_{\max}$), a minimum thrust procedure ($T_{\min}$), and a horizontal procedure (labeled HO). Whenever they are active, these procedures are formulated as equality constraints, so that a differential algebraic equation system is formed. The AM represents whether the aircraft is below (Be) or above (Ab) the tropopause, $h = 11.000$ m. The international standard atmosphere (ISA) model considers a piecewise defined relation $T(h)$, whose truncation takes place at the tropopause. Therefore, a discrete mode must be added to take it into consideration. This mode takes two values, $\mathrm{AM} \in \{\mathrm{Be}, \mathrm{Ab}\}$.

III. Case Studies

We carry out a comparison between fully procedured profiles, free-flight profiles, and optimized procedured profiles over short- and medium-range vertical flights.

A. Aircraft Continuous Dynamics

We consider a three-degree-of-freedom (DOF) dynamic model that describes the point variable-mass motion of the aircraft over a flat earth model. We assume a symmetric flight, with forces acting in the center of gravity and lying in the plane of symmetry. We neglect the thrust angle of attack. We consider the vertical motion of the aircraft, i.e., $\mathrm{DM} = \mathcal{V}$. A standard atmosphere is defined with $\Delta T_{\mathrm{ISA}} = 0$.

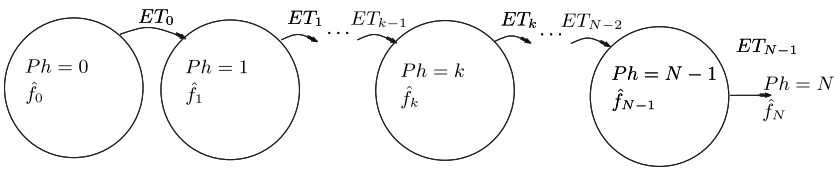

Fig. 1 Finite state machine for the flight plan model.

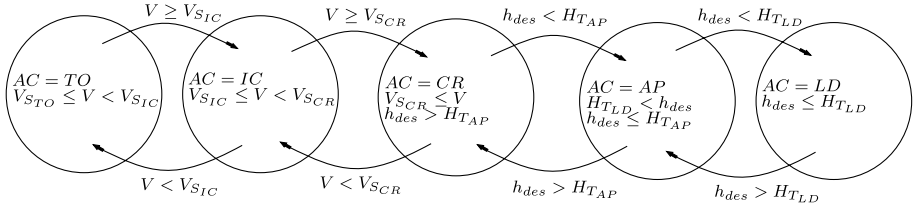

Fig. 2 Finite state machine for AC.

Table 1 A-320 ACs

Configuration	Flap	$C_{L_{\max}}$	C_{D_0}	C_{D_i}
TO	$1+F$	2.43	0.0393	0.0396
IC	1	2.19	0.0242	0.0469
CR	Clean	1.50	0.024	0.0375
AP	2	2.76	0.0456	0.0381
LD	Full	3.09	0.0838	0.0371

The coefficient of lift, $C_L = 2L/\rho S V^2$ (where L is the lift force, ρ the density of air, S the reference wing surface area, and V the true air speed), is, in general, a function of the angle of attack, α, and the Mach number, M, i.e., $C_L = C_L(\alpha, M)$. C_L is used as a control variable rather than the angle of attack. We assume a parabolic drag polar, i.e., $C_D = C_{D_0} + C_{D_i} C_L^2$, where C_{D_0} is the parasite coefficient and C_{D_i} is the induced coefficient. Eurocontrol base of aircraft data (BADA) 3.6 is used as the aircraft performance model [20]. These hypotheses lead to the following set of ODEs for aircraft performance:

$$m\dot{V} = T - D - mg\sin\gamma, \qquad mV\dot{\gamma} = L - mg\cos\gamma$$
$$\dot{x} = V\cos\gamma, \qquad \dot{h} = V\sin\gamma, \qquad \dot{m} = -\eta T \tag{13}$$

where the thrust, T, and C_L are the control inputs, and the true airspeed, V, the distance, x, the altitude, h, the flight-path angle, γ, and the mass of the aircraft, m, are the state variables. η refers to the thrust specific fuel flow. $D = C_D \frac{1}{2}\rho S V^2$ is the drag force.

We consider a BADA 3.6 Airbus A-320 model [20]. The different ACs and the value of aerodynamic parameters are listed in Table 1. The path constraints of the problem are those that define the aircraft's flight envelope. The maximum coefficient of lift, $C_{L_{\max_k}}$, the stall speed, V_{S_k}, and the thresholds, H_{T_k}, for $k = 0, \ldots, N$, vary depending on AC. The rest of constraints are the same for all phases:

$$0 \le h \le \min[H_{T_k}, h_{M0}, h_u], \qquad C_{V_{\min}} V_{S_k} \le V \le V_{Mo}$$
$$M \le M_{M0}, \qquad m_{\min} \le m \le m_{\max}, \qquad 0 \le C_L \le C_{L_{\max_k}}$$
$$T \le T_{\max}, \qquad \dot{m}_{\min} \le \dot{m} \tag{14}$$

where h_{M0} is the maximum operating altitude, h_u is the maximum dynamic altitude $[h_u = h_{\max} + G_t(\Delta T_{\mathrm{ISA}} - C_{Tc,4}) + G_W(m_{\max} - m)$, where $h_{\max}$ is the maximum altitude at maximum takeoff weight under ISA conditions, G_t is the temperature gradient on maximum altitude, ΔT_{ISA} is the temperature deviation from ISA, $C_{Tc,4}$ is the fourth thrust temperature coefficient, G_W is the mass gradient on maximum altitude, and $m_{\max}$ is the maximum mass of the aircraft], $C_{V_{\min}} = 1.3$ (except for TO, where $C_{V_{\min}} = 1.2$) is the minimum speed coefficient, V_{M_0} is the maximum operating calibrated airspeed, M_{M_0} is the maximum operating Mach number, $m_{\min}$ is the minimum aircraft mass, $T_{\max}$ is the maximum thrust, and $\dot{m}_{\min}$ is the minimum fuel flow. Values and formulas can be checked out in the BADA database manual [20].

Current instrumental landing systems (ILS) set the constant descent path between -2.5 and -3.5 deg, generally -3 deg. Therefore, regarding the landing phase, γ has also been constrained according to the typical values of an aircraft's final descent path, i.e.,

$$-6 \le \gamma_{\mathrm{Landing}} \le -2 \ \text{deg} \tag{15}$$

Notice that constraint (15) only applies for optimized procedured profiles; free-flight profiles do not have a specific constraint in the landing phase regarding γ.

B. Profiles Definition

Fully procedured profiles reflect the current ATM paradigm and have been defined accurately according to typical vertical profiles currently being flown. Those profiles can be found in BADA [20]. Modeling typical profiles in such a way enforces the specification of

Table 2 Short-range fully procedured flight profile

Phase	Name	AC	ET	OP	OC[a]
0	TO	TO	$V = 1.3V_{S_{\mathrm{IC}}}$	$T_{\max}$	$V_{\mathrm{CAS}} < 250$ kt
1	IC	IC	$V = 1.3V_{S_{\mathrm{CR}}}$	$T_{\max}$	$V_{\mathrm{CAS}} < 250$ kt
2	Res. free climb	CR	$h = 10,000$ ft	$T_{\max}$	$V_{\mathrm{CAS}} < 250$ kt
3	Climb accel	CR	$V_{\mathrm{CAS}} = 300$ kt	$h = 10,000$ ft, $T_{\max}$	——
4	Climb CAS	CR	Mach $= 0.78$	CAS $= 300$ kt, $T_{\max}$	——
5	Climb Mach	CR	$h = FL320$	$M = 0.78$, $T_{\max}$	——
6	Cruise	CR	——	$h = FL320$, $M = 0.78$	——
7	Descent Mach	CR	$V_{\mathrm{CAS}} = 300$ kt	$M = 0.78$, $T_{\min}$	——
8	Descent CAS	CR	$h = 10,000$ ft	CAS $= 300$ kt, $T_{\min}$	——
9	Descent decel	CR	$V_{\mathrm{CAS}} = 250$ kt	$h = 10,000$ ft, $T_{\min}$	——
10	Res. free descent	CR	$h = 6000$ ft	$T_{\min}$	$V_{\mathrm{CAS}} < 250$ kt
11	Approach	AP	$h = 2000$ ft.	PATH $= -3$ deg	$V_{\mathrm{CAS}} < 250$ kt
12	Landing	LD	Final cond.	PATH $= -3$ deg	$V_{\mathrm{CAS}} < 250$ kt

[a]OC refers to operational constraints due to operations near airports.

Table 3 Medium-range fully procedured flight profile

Phase	Name	AC	ET	OP	OC
0	TO	TO	$V = 1.3V_{S_{\mathrm{IC}}}$	$T_{\max}$	$V_{\mathrm{CAS}} < 250$ kt
1	IC	IC	$V = 1.3V_{S_{\mathrm{CR}}}$	$T_{\max}$	$V_{\mathrm{CAS}} < 250$ kt
2	Res. free climb	CR	$h = 10,000$ ft	$T_{\max}$	$V_{\mathrm{CAS}} < 250$ kt
3	Climb accel	CR	$V_{\mathrm{CAS}} = 300$ kt	$h = 10,000$ ft, $T_{\max}$	——
4	Climb CAS	CR	Mach $= 0.78$	CAS $= 300$ kt, $T_{\max}$	——
5	Climb Mach	CR	$h = FL360$	$M = 0.78$, $T_{\max}$	——
6	Cruise	CR	——	$h = FL360$, $M = 0.78$	——
7	Descent Mach	CR	$V_{\mathrm{CAS}} = 300$ kt	$M = 0.78$, $T_{\min}$	——
8	Descent CAS	CR	$h = 10,000$ ft	CAS $= 300$ kt, $T_{\min}$	——
9	Descent decel	CR	$V_{\mathrm{CAS}} = 250$ kt	$h = 10,000$ ft, $T_{\min}$	——
10	Res. free descent	CR	$h = 6000$ ft	$T_{\min}$	$V_{\mathrm{CAS}} < 250$ kt
11	Approach	AP	$h = 2000$ ft.	PATH $= -3$ deg	$V_{\mathrm{CAS}} < 250$ kt
12	Landing	LD	Final cond.	PATH $= -3$ deg	$V_{\mathrm{CAS}} < 250$ kt

Table 4 Short-range optimized procedured flight profile

Phase	Name	AC	ET	OP	OC
0	TO	TO	$V = 1.3V_{S_{IC}}$	——	$V_{CAS} < 250$ kt
1	IC	IC	$V = 1.3V_{S_{CR}}$	——	$V_{CAS} < 250$ kt
2	Res. free climb	CR	$h = 10,000$ ft	——	$V_{CAS} < 250$ kt
3	Climb accel	CR	——	$h = 10,000$ ft	——
4	Climb CAS	CR	——	CAS, T_{max}	——
5	Climb Mach	CR	——	M, T_{max}	——
6	Cruise	CR	——	HO	——
7	Descent Mach	CR	——	M	——
8	Descent CAS	CR	$h = 10,000$ ft	CAS	——
9	Descent decel	CR	——	$h = 10,000$ ft	——
10	Res. free descent	CR	$h = 6000$ ft	T_{min}	$V_{CAS} < 250$ kt
11	Approach	AP	$h = 2000$ ft	PATH	$V_{CAS} < 250$ kt
12	Landing	LD	Final cond.	PATH	$V_{CAS} < 250$ kt

two operative procedures per phase, for instance, to climb with constant calibrated air speed (V_{CAS}) and constant throttle setting, or to perform a steady cruise, i.e., with defined constant Mach and constant altitude.

Free-flight profiles are defined by combining some velocity constraints due to airports terminal area restrictions, together with an enroute free-flight performance. Such profiles are considered as optimal benchmark and represent a comparison baseline, being useful for a better understanding of optimal performances and a quantitative analysis of current inefficiencies.

Optimized procedured profiles are defined seeking a short-term more efficient use of the current ATM paradigm based on TBO. The enroute imposed procedures are derived from a better air traffic control and ATM instead of a pure enroute free flight. They are based on a relaxation of current procedures, by setting, in general, just one procedure per phase, and also relaxing some capture conditions for switching. Referring the reader to Tables 2 and 3, it can be observed that the optimized procedured profiles are defined with some trigger conditions, the so-called capture conditions for switching. When this occur, the switchings are autonomous, e.g., they occur when the aircraft reaches the respective altitudes or velocities. On the contrary, switches between phases with noncapture conditions are called controlled switches since they are given by the control law within the optimal solution. It is easy to see that the main difference between fully procedured and optimized procedured profiles is, together with less restricted procedures, the fact that some controlled switches are allowed. As a consequence, the transition Mach, the cruising altitude, or the constant calibrated speed of descent are not prefixed, but are set by the optimal solution, leading the system to an overall minimum fuel consumption.

Table 5 Short-range free-flight profile

Phase	Name	AC	ET	OP	OC
0	TO	TO	$V = 1.3V_{S_{IC}}$	——	$V_{CAS} < 250$ kt
1	IC	IC	$V = 1.3V_{S_{CR}}$	——	$V_{CAS} < 250$ kt
2	Res. free climb	CR	$h = 10,000$ ft	——	$V_{CAS} < 250$ kt
3	Free CL/CR/DS	CR	$h = 10,000$ ft	——	——
4	Res. free descent	CR	$h = 6000$ ft	——	$V_{CAS} < 250$ kt
5	Approach	AP	$h = 2000$ ft	——	$V_{CAS} < 250$ kt
6	Landing	LD	Final cond.	——	$V_{CAS} < 250$ kt

1. *Short Range*

Tables 2, 4, and 5 show, respectively, the fully procedured, optimized procedured, and free-flight profiles herein used for numerical computation. The short-range fully procedured flight has been derived from a real Madrid–Oviedo flight plan following BADA-like flight procedures with airline-defined speed and altitude profile values [20]. The boundary conditions of the flight are the following: $x_{t_I} = 0$, $h_{t_I} = 0$, $v_{t_I} = 1.2V_{\text{stall}_{TO}}$ m/s, $\gamma_{t_I} = 0.05$ rad, $m_{t_I} = 63,070$ Kg; $x_{t_F} = 476$ km, $h_{t_F} = 0$.

2. *Medium Range*

Tables 3, 6, and 7 show, respectively, the fully procedured, optimized procedured, and free-flight profiles herein used for the numerical simulation. The medium-range fully procedured flight has been derived from a real Madrid–Berlin flight plan following BADA-like flight procedure with airline-defined speed and altitude profile values [20]. The boundary conditions of the flight are the following: $x_{t_I} = 0$, $h_{t_I} = 0$, $v_{t_I} = 1.2V_{\text{stall}_{TO}}$ m/s, $\gamma_{t_I} = 0.05$ rad, $m_{t_I} = 69,415$ Kg; $x_{t_F} = 2035$ km, $h_{t_F} = 0$.

IV. Experimental Results

The fully procedured profile computations have been carried out using a tool combining three-DOF flight dynamics differential equations with procedure-oriented three-dimensional flight control. More precisely, the aircraft ODE system Eq. (13) with the same performance based on BADA and atmosphere models (ISA) is integrated using the set of path constraints (14), while controls are

Table 6 Medium-range optimized procedured flight profile

Phase	Name	AC	ET	OP	OC
0	TO	TO	$V = 1.3V_{S_{IC}}$	——	$V_{CAS} < 250$ kt
1	IC	IC	$V = 1.3V_{S_{CR}}$	——	$V_{CAS} < 250$ kt
2	Res. free climb	CR	$h = 10,000$ ft	——	$V_{CAS} < 250$ kt
3	Climb accel	CR	——	$h = 10,000$ ft	——
4	Climb CAS	CR	——	CAS, T_{max}	——
5	Climb Mach	CR	——	M, T_{max}	——
6	Cruise	CR	——	HO	——
7	Descent Mach	CR	——	M	——
8	Descent CAS	CR	$h = 10,000$ ft	CAS	——
9	Descent decel	CR	——	$h = 10,000$ ft	——
10	Res. free descent	CR	$h = 6000$ ft	T_{min}	$V_{CAS} < 250$ kt
11	Approach	AP	$h = 2000$ ft	PATH	$V_{CAS} < 250$ kt
12	Landing	LD	Final cond.	PATH	$V_{CAS} < 250$ kt

Table 7 Medium-range free-flight profile

Phase	Name	AC	ET	OP	OC
0	TO	TO	$V = 1.3V_{S_{IC}}$	——	$V_{CAS} < 250$ kt
1	IC	IC	$V = 1.3V_{S_{CR}}$	——	$V_{CAS} < 250$ kt
2	Res. free climb	CR	$h = 10,000$ ft	——	$V_{CAS} < 250$ kt
3	Free CL/CR/DS	CR	$h = 10,000$ ft	——	——
4	Res. free descent	CR	$h = 6000$ ft	——	$V_{CAS} < 250$ kt
5	Approach	AP	$h = 2000$ ft	——	$V_{CAS} < 250$ kt
6	Landing	LD	Final cond.	——	$V_{CAS} < 250$ kt

properly set using a flight management system so that the aircraft follows the given flight procedures.

Optimized procedured and free-flight profiles are defined and formulated according to Sec. II. To solve the resulting optimal control problem, Eqs. (7–12), a Hermite–Simpson collocation method [21] has been used. The so-called collocation methods are based on interpolating both control and state variables by means of some piecewise continuous functions. The time domain is split into smaller subintervals. In each subinterval, the variables of the equivalent nonlinear programming (NLP) problem are the values of states and controls at the extremes of the subinterval and at the collocation point. The state variables are approximated by piecewise cubic polynomial functions. A linear interpolation is used for controls. The set of ODEs is replaced by a finite set of equality constraints, the so-called defect equations. Notice that derivatives of discretized state and constraint functions are obtained by finite difference estimates, so that it is not necessary to analytically derive them. The resulting sparse NLP has been solved using IPOPT [22]. IPOPT showed robustness in solving infeasible subproblems in the iterative process even when dealing with infeasible initial guesses. IPOPT showed also robustness when dealing with different initial conditions, showing similar results patterns. Both optimized procedured and free-flight profiles have a discretization grid with $n = 650$ ($n_1 = n_2 = \ldots n_{13} = 50$) sample points. In the free-flight profiles, for the sake of comparison, the fourth phase is composed of 350 discrete states. Fully procedured profiles are computed in real time with samples every second. To illustrate computational issues, in the medium-range optimized procedured case, the resulting NLP had 4299 variables, 3597 equality constraints, and 4151 inequality constraints. The total computational time on a 2.56 GHz laptop with 4 GB RAM was 1369.86 s.

Tables 8 and 9 show, respectively, the short- and medium-range flight results: they contain the total flight times and times of switching when applied (t_k s), the consumptions including the accumulate consumption at the end of every phase when applied (C_k kg), and the constant values that describe the optimized aircraft performance in the different flight procedures (value opt).

Note that the algorithm neglects the inefficient phases. In this case, phases 7 and 9, descent Mach and descent deceleration, are eliminated by the optimal solution by setting the corresponding durations to zero, i.e., setting equal switching times. In this manner, the algorithm for optimized procedured profiles leads the aircraft to what would be a CDA.

Controls, states, and optimal switching instants are represented, respectively, for short and medium range, in Figs. 3 and 4. Notice that since the patterns of the solutions for both short and medium range are very similar, for the sake of space, Fig. 3 contains only the representative variables, h, V, and γ. Regarding the state variables, in general, except for the case of γ (Figs. 3c and 4c), all state variables vary smoothly. γ exhibits high-frequency dynamics at some points near the switchings. This suggests discontinuity around those points. Notice that this behavior is normal since the purpose here is not to

Table 8 Short-range results

Phase[a]	t, s[b]	t_k, s[c]	t_k, s[d]	C, kg[b]	C_k, kg[c]	C_k, kg[d]	Value opt
0	——	8.69	8.69	——	18.16	18.16	Free
1	——	25.04	25.06	——	52.94	52.96	Free
2	——	225.3	225.38	——	441.44	441.57	Free
3	——	249.41	——	——	482.71	——	$h = 10,000$ ft
4	——	755.409	——	——	1161.36	——	$V_{CAS} = 150.459$ [m/s] & T_{max}
5	——	1193.11	——	——	1550.29	——	Mach $= 0.7297$ & T_{max}
6	——	1243.9	——	——	1554.87	——	$h = 10875.4$ m
7	——	1243.9	——	——	1554.87	——	Mach $= 0.6422$
8	——	2416.84	——	——	1681.77	——	$V_{CAS} = 108.406$ m/s
9	——	2416.84	2368.83	——	1681.77	1661.55	$h = 10,000$ ft
10	——	2677.17	2642.83	——	1716.68	1698.26	T_{min}
11	——	2826.22	2853.54	——	1737.66	1728.08	$\gamma = -4.3911$ deg
12	2592.8	2922.08	2942.26	1967.15	1752.71	1741.09	$\gamma = -4.3911$ deg

[a]Corresponds to optimized procedured profile phases. For free-flight profile, number 9 corresponds to phase 3 (free CL/CR/DS), etc.
[b]Corresponds to fully procedured profiles.
[c]Corresponds to optimized procedured profiles.
[d]Corresponds to free-flight profiles.

Table 9 Medium-range results[a]

Phase	t, s	t_k, s	t_k, s	C, kg	C_k, kg	C_k, kg	Value opt
0	——	11.61	11.61	——	24.26	24.26	Free
1	——	33.28	33.29	——	70.25	70.27	Free
2	——	254.66	254.71	——	498.50	498.58	Free
3	——	287.89	——	——	555.43	——	$h = 10,000$ ft
4	——	796.57	——	——	1258.31	——	$V_{CAS} = 154.817$ [m/s] & T_{max}
5	——	1653.76	——	——	1995.43	——	Mach $= 0.7249$ & T_{max}
6	——	7774.07	——	——	6034.37	——	$h = 11295.4$ m
7	——	7774.08	——	——	6034.38	——	Mach $= 0.6772$
8	——	8964.12	——	——	6161.77	——	$V_{CAS} = 111.138$ m/s
9	——	8964.12	8929.65	——	6161.77	6068.77	$h = 10,000$ ft
10	——	9222.08	9184.45	——	6196.36	6102.95	T_{min}
11	——	9369.81	9388.6	——	6217.16	6131.87	$\gamma = -4.3823$ deg
12	9403.5	9464.6	9475.87	6529.85	6231.05	6144.66	$\gamma = -4.3823$ deg

[a]Interpretation holds the same as in Table 8.

capture short duration maneuvers, for which we would need a coarser discretization around the switchings. Figures 4e and 4f show the behavior of control inputs for medium range. The optimized procedured profile controls show some bang-bang behavior near the switchings. Free-flight controls show, however, a smoother behavior. For short range the behavior is similar.

Results show that the proposed optimized procedured profiles save, respectively, for short and medium range, 10.9 and 4.6% of fuel consumption, i.e, 214.44 and 298.8 kg, respectively, when compared to fully procedured profiles. Furthermore, results also show that free-flight profiles achieve, respectively, 11.5 and 5.9%, i.e., 226.06 and 385.19 kg, respectively, of fuel savings when compared to fully procedured profiles. This means that optimized procedured profile efficiency is very close to the considered optimal benchmark.

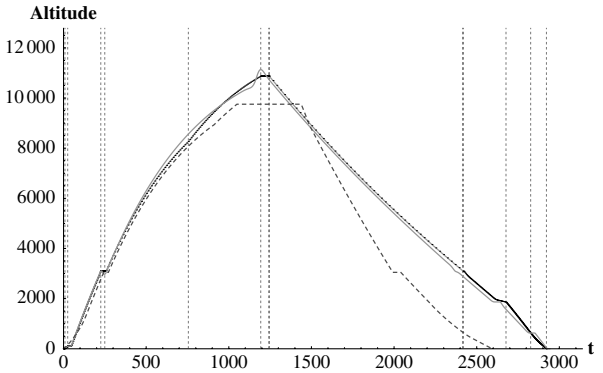

a) t-h

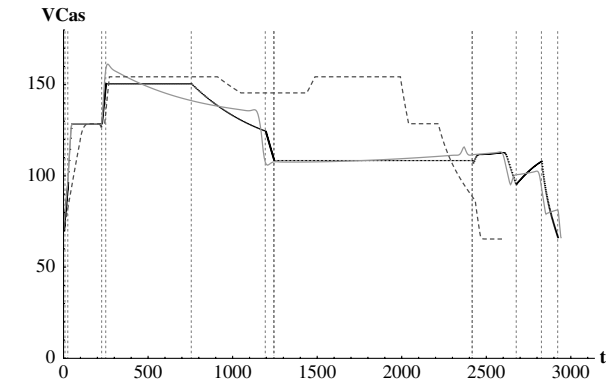

b) t-V_{CAS}

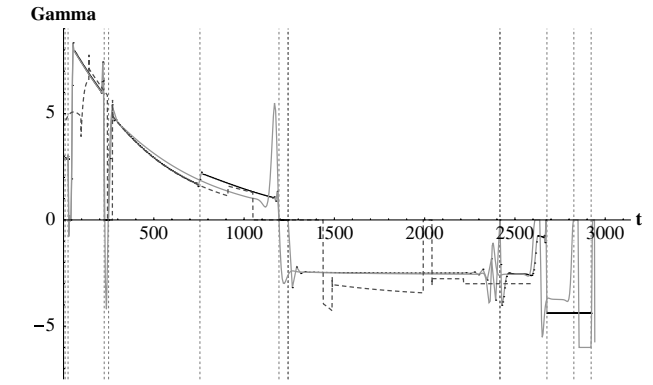

c) t-γ

Fig. 3 Short-range, h, V_{CAS}, and γ: dashed line corresponds to fully procedured profile; solid dotted line corresponds to optimized-procedured profile (being the dots of the computed sample points); solid dotted line corresponds to free-flight profile. Note that the depicted vertical dashed lines correspond to the optimized procedured profile switching times.

V. Discussion of Results

A. Short Range

We first analyze free-flight performances. In the optimum solution of the free flight the aircraft seeks to achieve maximum altitude in minimum time, since flying at low altitudes with maximum thrust setting is very fuel consuming. As the aircraft gets higher, it progressively softens its rate of climb until it suddenly performs a sharp climb maneuver to intercept the optimum descent path, thus skipping the cruise phase. With this maneuver, the aircraft consumes the excessive speed with respect to the optimum descent speed, while enabling an anticipated interception of the optimum descent path thanks to the fast altitude gain. Otherwise, the climb would last longer, resulting in greater fuel consumption. The optimum descent path is the result of descending at maximum gradient speed, which allows the aircraft to fly the greatest distance possible at idle thrust, thus minimizing fuel consumption. This optimum speed is the minimum drag speed, also known as base speed. This speed decreases as air density increases, so the aircraft lowers its speed as it descends. The base speed also changes as the aircraft deploys high-lift devices, so the aircraft speed is adjusted by regulating the flight-path angle when a change in AC is to be performed. At the very end of the flight, when the only aim is to land at any flyable speed, the flight-path angle is increased to cover the greatest distance possible before touching ground, consuming the excess of speed above minimum speed.

There are two main differences when performing the descent between fully procedured and free-flight profiles. The first one is that fully procedured flights descend at a speed much higher than the base speed (300 vs 210 kt). This permits fully procedured flights to reduce flight duration at the cost of increasing fuel consumption. The second difference is that fully procedured flights perform the approach at the ILS -3 deg glide path. When the approach glide path is less inclined than the maximum gradient path (as in this case), the glide path becomes too low for the aircraft to maintain the desired speed at idle thrust. Thus, some extra thrust is required during the approach, resulting in increased fuel consumption.

In the solution of the optimized procedured profiles, the aircraft tries always to follow the patterns of free-flight optimal performance, fulfilling some prefixed procedures. Consequently, it seems that the algorithm aims to minimize climb phase duration since it is very fuel consuming, but at the same time it needs to prevent negative effects on the optimality of the subsequent flight phases. The obtained 292 kt/0.73 climb speed is similar to the fully procedured profile in the constant CAS phase but shows a significantly lower speed for the constant Mach phase because it provides a higher rate of climb. Then the aircraft performs a short cruise (4 s). This is the duration needed to decelerate from the climbing velocity to the descending one. The aircraft intercepts the descending path, performing it at 108 m/s (CAS), 211 kt approximately, considerably different than the fully procedured 300 kt. This is optimal thanks to the minimum drag CAS being almost constant along the descent, consequently neglecting the constant Mach phase. Finally, the constant flight-path angle of initial and final approach, -4.39 deg, is more inclined than the fully procedured one, -3 deg.

B. Medium Range

As in the previous case, medium-range optimum free flight seeks to achieve maximum altitude in minimum time. As the aircraft gets higher, it progressively reduces its rate of climb to make a smooth transition to the subsequent pseudocruise phase, in which the aircraft asymptotically approaches its operating ceiling. The optimization target during cruise is to maximize the specific range, which is the distance traveled per unit of fuel consumed. As the aircraft mass decreases due to fuel burn, the optimum profile shows an increasing trend in altitude following the also increasing operating ceiling, while speed is conveniently adjusted, typically in a slightly decreasing trend. Such a performance is known as continuous cruise climb. Cruise phase ends when the optimum descent path is intercepted. For the optimum descent path, it states the principles of free optimal performance explained for short-range flights.

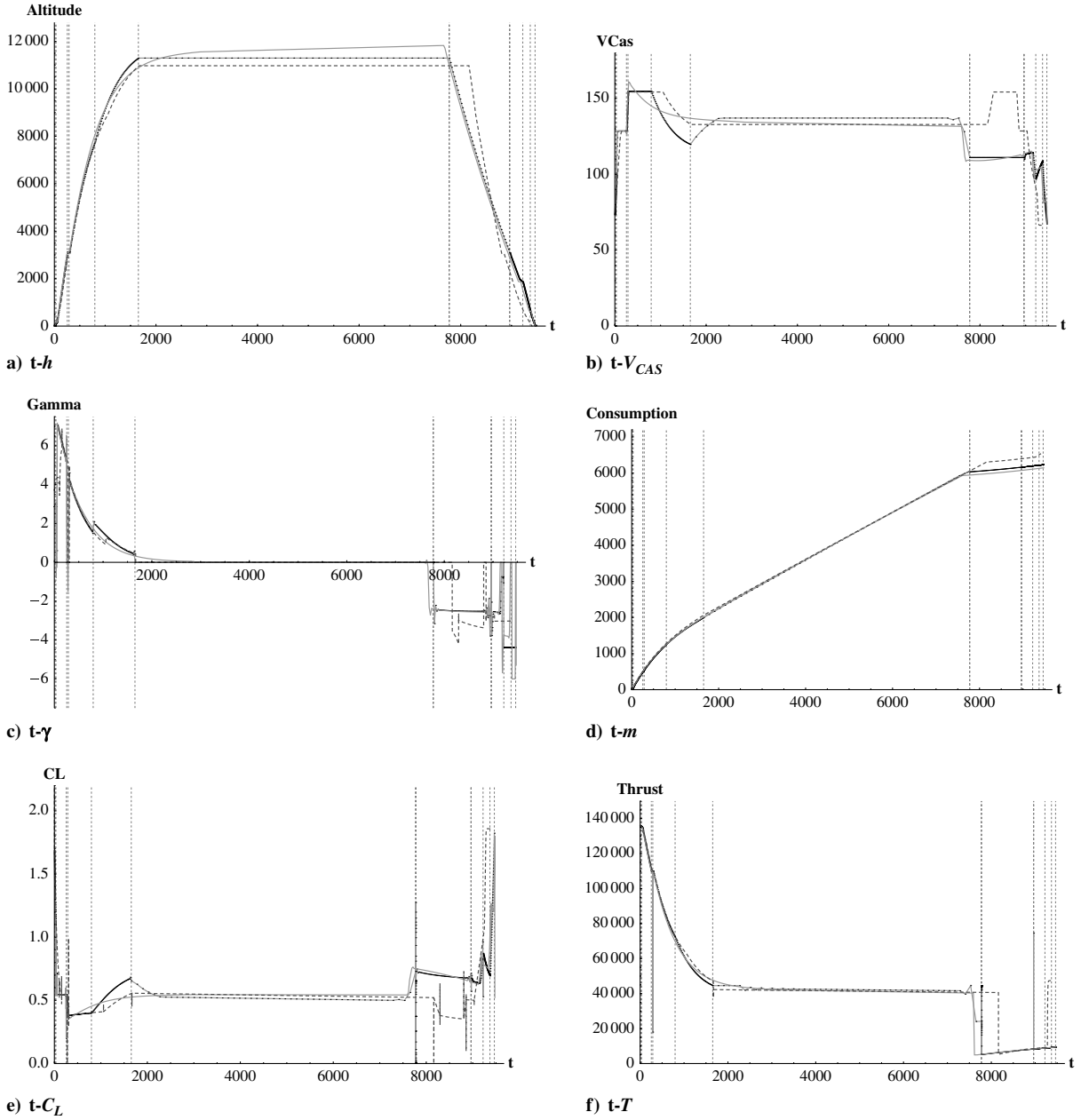

Fig. 4 Medium-range, h, V_{CAS}, consumption, γ, and control laws, T and C_L: dashed line corresponds to fully procedured profile; solid dotted line corresponds to optimized procedured profile (being the dots of the computed sample points); solid dotted line corresponds to free-flight profile. Note that the depicted vertical dashed lines correspond to the optimized procedured profile switching times.

Again, as pointed out for the short-range flights, the optimized procedured profile tries always to follow the patterns of free-flight optimal performance. The obtained 301 kt/0.72 climb shows a significantly lower speed for the constant Mach phase. Then the aircraft performs the cruise at an altitude that is limited by the operating ceiling at the beginning of cruise (where the ceiling is lower due to the greater mass). Eventually, the aircraft intercepts the descending path, performing it at 111 m/s (CAS), 215 kt approximately. Finally, the constant flight-path angle of initial and final approach, −4.38 deg, is more inclined than the typical one, −3 deg. Notice that a closer performance to free-flight continuous cruise climb could have been achieved by defining at least one step climb.

C. General Remarks

Whereas some differences exist in ascent and cruise, the key differences of performance between current and future concepts of operations arise in descent phases, where indeed descent velocity and ILS arrival flight-path angle exhibit high deviations from what has been shown as the optimal benchmark: to descend at the base velocity and to perform approach and landing at the maximum gradient path.

Focusing on descent, we should consider separately the track going from the top of descent to the initial approach fix and the track going from that fix to the runway. The first track could be improved without operational problems by just following the profile given by the maximum gradient velocity at idle thrust. Lacking that, a constant CAS procedure around the average base velocity could be defined, which as it has been said is not far from the optimal benchmark. The main reason that current flights use a constant CAS up to 300 kt is to reduce descent duration. Regarding final and initial approach, it does not seem to be easily achievable to perform the obtained results. The free-flight optimal path shows a very steep path, while performing landing with quasi-level flight. This profile is unsafe because descent paths are designed as a tradeoff between obstacle avoidance handling and nonexcessive descent rates. Free-flight profiles shows rather high descent rates followed by a potentially nonhandling obstacles horizontal path. Optimized procedured profile descent paths showed, however, higher than current ILS constant path angles, closer to the

optimal benchmark path, avoiding also potential obstacles. Such paths would lead to higher descent rates, but lower than free-flight descent paths. The paradigm of the global navigation satellite system descent procedures will help defining ad hoc descent paths within safety standards, and, thus, some of the preceding obtained fuel savings could be achieved.

It is necessary to point out that the BADA aerodynamic model does not take into account compressibility effects on the aerodynamic behavior of the aircraft. This leads to lower-than-real drag at high-Mach numbers, resulting in higher-than-real optimum speeds and altitudes.

VI. Conclusions

The proposed method to generate the optimized procedured profiles provides a powerful framework to design flexible flight plans by defining less restricted procedures. Fuel savings achieved coincide with the ones expected by SESAR (300–500 kg per flight on average). Thus, this approach provides a tool to plan flights with much less consumption than current ones, close to the free-flight optimal benchmark performance. This framework is suitable to formulate a multicriteria multiphase optimal control problem in which noise, emissions, or global warming effects could be also included.

The results show that some current phases, such as descent Mach and descent deceleration, are clearly inefficient. The algorithm showed consistency when dealing with such inefficient phases and was capable of neglecting them, leading to CDA optimal descent performance.

Acknowledgments

This work is partially supported by the Spanish Government through the Ministerio de Ciencia e Innovación, the Comunidad de Madrid, the project i-Math Ingenio Mathematica, and the project Optimización en Computación en Paralelo de Planificación bajo Incertidumbre under grant no. MTM2009-14087-C04-01. This work has been carried out within the framework of the Atlantida project, partially funded by the Spanish Centro para el Desarrollo Tecnológico e Industrial, in which the Universidad Rey Juan Carlos collaborated with GMV Aerospace and Defence S.A.

References

[1] SESAR Consortium, "Air Transport Framework: The Current Situation, SESAR Definition Phase Milestone Deliverable 1," July 2006.

[2] SESAR Consortium, "SESAR Master Plan, SESAR Definition Phase Milestone Deliverable 5," April 2008.

[3] SESAR Joint Undertaking, "BROCHURE 02 Q4 2009," Responsible Editor Patrick Ky.

[4] Saez, F., García, E., and Schaefer, D., "Introduction to the SESAR WP E Research Network: HALA! (Higher Automation Levels in ATM)," Paper EN-114, ENRI International Workshop on ATM/CNS, Tokyo, 2010.

[5] SESAR Consortium, "The ATM Target Concept, SESAR Definition Phase Milestone Deliverable 3," Sept. 2007.

[6] Betts, J. T., and Cramer, E. J., "Application of Direct Transcription to Commercial Aircraft Trajectory Optimization," *Journal of Guidance, Control, and Dynamics*, Vol. 18, No. 1, Jan.–Feb. 1995, pp. 151–159. doi:10.2514/3.56670

[7] Ringertz, U., "Aircraft Trajectory Optimization as a Wireless Internet Application," *Journal of Aerospace Computing, Information, and Communication*, Vol. 1, No. 2, 2004, pp. 85–99. doi:10.2514/1.1279

[8] Norsell, M., "Multistage Trajectory Optimization with Radar-Range Constraints," *Journal of Aircraft*, Vol. 42, No. 4, 2005, pp. 849–857. doi:10.2514/1.8544

[9] Soler, M., Olivares, A., and Staffetti, E., "Hybrid Optimal Control Approach to Commercial Aircraft Trajectory Optimization," *Journal of Guidance, Control, and Dynamics*, Vol. 33, No. 3, May–June 2010, pp. 985–991. doi:10.2514/1.47458

[10] Visser, H., and Wijnen, R., "Optimization of Noise Abatement Departure Trajectories," *Journal of Aircraft*, Vol. 38, No. 4, 2001, pp. 620–627. doi:10.2514/2.2838

[11] Torres, R., Chaptal, J., Bes, C., and Hiriart-Urruty, J., "Optimal, Environmentally Friendly Departure Procedures for Civil Aircraft," *Journal of Aircraft*, Vol. 48, No. 1, Jan.–Feb. 2011, pp. 11–22. doi:10.2514/1.C031012

[12] Houacine, M., and Khardi, S., "Gauss Pseudospectral Method for Less Noise and Fuel Consumption from Aircraft Operations," *Journal of Aircraft*, Vol. 47, No. 6, Nov.–Dec. 2010, pp. 2152–2159. doi:10.2514/1.C031007

[13] Prats, X., Puig, V., and Quevedo, J., "Equitable Aircraft Noise-Abatement Departure Procedures," *Journal of Guidance, Control, and Dynamics*, Vol. 34, No. 1, 2011, pp. 192–203. doi:10.2514/1.49530

[14] Pargett, D. M., and Ardema, M. D., "Flight Path Optimization at Constant Altitude," *Journal of Guidance, Control, and Dynamics*, Vol. 30, No. 4, 2007, pp. 1197–1201. doi:10.2514/1.28954

[15] Franco, A., Rivas, D., and Valenzuela, A., "Minimum-Fuel Cruise at Constant Altitude with Fixed Arrival Time," *Journal of Guidance, Control, and Dynamics*, Vol. 33, No. 1, 2010, pp. 280–285. doi:10.2514/1.46465

[16] Clarke, J.-P. B., Ho, N. T., Ren, L., Brown, J. A., Elmer, K. R., Tong, K.-O., and Wat, J. K., "Continuous Descent Approach: Design and Flight Test for Louisville International Airport," *Journal of Aircraft*, Vol. 41, No. 5, 2004, pp. 1054–1066. doi:10.2514/1.5572

[17] Dinges, E., "Determining the Environmental Benefits of Implementing Continuous Descent Approach Procedures," Paper 017, Seventh USA/Europe Seminar on Air Traffic Management Research and Development (ATM2007), Barcelona, 2–5 July 2007.

[18] Shresta, S., N. D., and Williams, S. S., "Analysis of Continuous Descent Benefits and Impacts During Daytime Operations," Paper 132, Eighth USA/Europe Seminar on Air Traffic Management Research and Development (ATM2009), Napa, CA, 29 June –2 July 2009.

[19] Jacobsen, M., and Ringertz, U., "Airspace Constraints in Aircraft Emission Trajectory Optimization," *Journal of Aircraft*, Vol. 47, No. 4, 2010, pp. 1256–1265. doi:10.2514/1.47109

[20] Nuic, A., "User Manual for the Base of Aircraft Data (BADA) Revision 3.6," Eurocontrol Experimental Center, 2005.

[21] Hargraves, C. R., and Paris, S. W., "Direct Trajectory Optimization Using Nonlinear Programming and Collocation," *Journal of Guidance, Control, and Dynamics*, Vol. 10, No. 4, 1987, pp. 338–342. doi:10.2514/3.20223

[22] Wächter, A., and Biegler, L., "On the Implementation of an Interior-Point Filter Line-Search Algorithm for Large-Scale Nonlinear Programming," *Mathematical Programming*, Vol. 106, No. 1, 2006, pp. 25–57. doi:10.1007/s10107-004-0559-y